AGU PUBLICATIONS

Paleoceanography

RESEARCH ARTICLE
10.1002/2015PA002870

Key Points:
- SPCZ migrated and/or intensified since 3200 years B.P. in response to orbital forcing
- Enhanced South Pacific (SP) cyclogenesis occurred between ~2600 and 1500 years B.P.
- Changes in SP rainfall ~1000 years B.P. may have prompted Polynesian expansion

Supporting Information:
- Supporting Information S1

Correspondence to:
M. R. Toomey,
mrt02008@gmail.com

Citation:
Toomey, M. R., J. P. Donnelly, and J. E. Tierney (2016), South Pacific hydrologic and cyclone variability during the last 3000 years, *Paleoceanography*, *31*, 491–504, doi:10.1002/2015PA002870.

Received 8 AUG 2015
Accepted 26 MAR 2016
Accepted article online 31 MAR 2016
Published online 18 APR 2016

South Pacific hydrologic and cyclone variability during the last 3000 years

Michael R. Toomey[1,2,3], Jeffrey P. Donnelly[2], and Jessica E. Tierney[2,4]

[1]Jackson School of Geosciences, University of Texas at Austin, Austin, Texas, USA, [2]Department of Geology and Geophysics, Woods Hole Oceanographic Institution, Woods Hole, Massachusetts, USA, [3]Department of Earth, Atmospheric and Planetary Sciences, Massachusetts Institute of Technology, Cambridge, Massachusetts, USA, [4]Department of Geosciences, University of Arizona, Tucson, Arizona, USA

Abstract Major excursions in the position of the South Pacific Convergence Zone (SPCZ) and/or changes in its intensity are thought to drive tropical cyclone (TC) and precipitation variability across much of the central South Pacific. A lack of conventional sites typically used for multimillennial proxy reconstructions has limited efforts to extend observational rainfall/TC data sets and our ability to fully assess the risks posed to central Pacific islands by future changes in fresh water availability or the frequency of storm landfalls. Here we use the sedimentary record of Apu Bay, offshore the island of Tahaa, French Polynesia, to explore the relationship between SPCZ position/intensity and tropical cyclone overwash, resolved at decadal time scales, since 3200 years B.P. Changes in orbital precession and Pacific sea surface temperatures best explain evidence for a coordinated pattern of rainfall variability at Tahaa and across the Pacific over the late Holocene. Our companion record of tropical cyclone activity from Tahaa suggests major storm activity was higher between 2600-1500 years B.P., when decadal scale SPCZ variability may also have been stronger. A transition to lower storm frequency and a shift or expansion of the SPCZ toward French Polynesia around 1000 years B.P. may have prompted Polynesian migration into the central Pacific.

1. Introduction

The South Pacific Convergence Zone (SPCZ) is a convective rain trough that stretches across the South Pacific with its mean axis orientated from Solomon Islands to French Polynesia [*Vincent*, 1994; *Vincent et al*., 2011]. Northward migration and zonal orientation of the SPCZ, particularly during El Niño events, is thought to drive stronger cyclogenesis in the central South Pacific on interannual time scales by reducing wind shear around French Polynesia [*Revell and Goulter*, 1986; *Vincent et al*., 2011]. Observational records also link the behavior of the SPCZ to sea surface temperature (SST) anomalies associated with the Interdecadal Pacific Oscillation [*Folland et al*., 2002] and solar insolation [*Meehl et al*., 2009]. However, these inferred relationships are based on short data sets (<150 years) and may not be stationary in the recent geologic past.

Existing proxy records of past Pacific hydrologic variability [e.g., *Conroy et al*., 2008; *Moy et al*., 2002] demonstrate that precipitation patterns across the basin have varied on centennial to millennial time scales during the middle and late Holocene. In general, these records show increased rainfall variability since ~3000 years B.P. [*Donders et al*., 2008] but disagree on the detailed behavior of Pacific hydrographic variability since the mid Holocene. A key gap lies in the central Pacific—where at present, no continuous, high-resolution, multimillennial rainfall records exist—greatly limiting our ability to characterize climate dynamics that have occurred across the basin. The lack of paleoclimate data from this region is in part due to a scarcity of conventional paleoclimate archives, such as those from upland lakes. However, back-reef lagoons surrounding high volcanic islands occur throughout much of the central Pacific, and can offer detailed records of Pacific climate variability. On many reef-enclosed islands, deep lagoons (>30 m) occupy coastal embayments and capture terrestrial sediments [*Zinke et al*., 2001] likely shed by nearby slopes during runoff events. Such sites are widespread and have high potential as valuable paleoclimate archives. Previous coring and geophysical efforts indicate that deposition in back-barrier reef lagoons has been fast (up to 6.9 mm/yr) [*Montaggioni*, 2005] and spans much of the Holocene as well as previous interglacials [*Le Roy et al*., 2008].

Here we use sedimentary records of late Holocene tropical cyclone and SPCZ variability from Apu Bay, offshore the island of Tahaa, French Polynesia, to answer two main questions: (1) how is the SPCZ's position or strength impacted by different climatic regimes (e.g., SST, insolation) and (2) is there a statistically significant relationship between SPCZ behavior and tropical cyclone activity in the central South Pacific on geologic time scales?

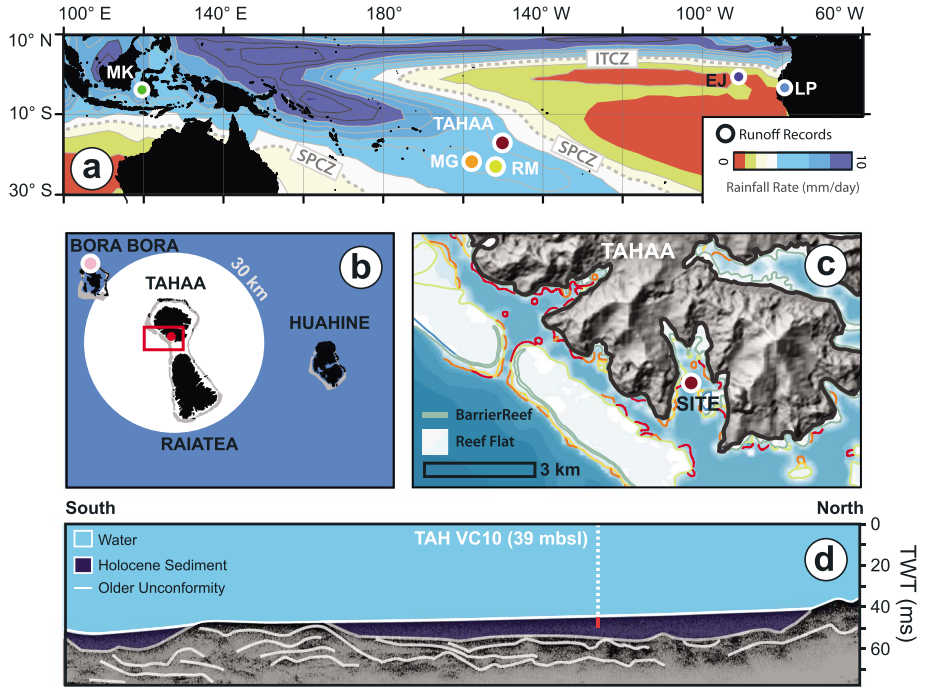

Figure 1. (a) Satellite (CMAP [*Xie and Arkin*, 1997]—NOAA/OAR/ESRL) observed precipitation over the past 30 years (1979–2009 C.E.). Circles indicate locations of climate records used in Figures 5 and 6: Makassar Strait (MK, green), Tahaa (red), Mangaia (orange), Rimatara (yellow), Laguna Pallcacocha (LP, light blue), and El Junco (EJ, dark blue). (b) Location of Tahaa relative to other islands in the Society Islands Chain. Position of rain gauge station on Bora Bora is shown by purple circle. Apu Bay and Bora Bora both sit in a slight rain shadow topographic highs on Tahaa (maximum elevation = 590 m) relative to the prevailing trade winds. (c) Topographic (Aster 30 m resolution) and bathymetric (British Admiralty chart #1103) map of southwestern Tahaa centered on Apu Bay, our coring site, TAH VC10. (d) Seismic trace running north-south through Apu Bay which shows deposition of a large wedge of Holocene sediment as well as several older reflectors. The location of TAH VC10 is indicated by a white dashed line.

2. Study Site

Tahaa is a highly eroded volcanic ocean island, formed 2–3 Myr ago [*Guillou et al*., 2005] as part of the Society Islands hotspot chain (Figures 1a and 1b). Apu Bay is ~40 m deep drowned valley incised into the volcanic upland and flanked on three sides by steep (~25 % grade) ridges (Figure 1c). Submerged karst, visible in aerial imagery of the barrier (16°41.241′S 151°29.648′W) fronting Apu Bay, suggests that the geometry of the site has not changed substantially since the glacial transgression. Core TAH VC10 (~3.8 m in length, including the core catcher) was taken in the center of the bay (39 m water depth), ~500 m from the shore (16°40.116′S, 151°29.508′W). Seismic surveying at the site (Figure 1d) and ^{14}C dating indicates that a large, relatively uniform sedimentary pile (shaded blue) has accumulated in Apu Bay since deglacial sea level inundation.

Tahaa is located on the southeastern edge of the modern SPCZ trough and experiences major seasonal as well as interannual changes in precipitation (Figures 2a and 2b). El Niño (La Niña) events are associated with a northeastern (southwestern) displacement of the SPCZ [*Widlansky et al*., 2011] and increased (decreased) precipitation at Tahaa. A rain gauge record from Bora Bora (38 km NW of our site) shows a ~30% increase in precipitation during months when the Southern Oscillation Index (www.cgd.ucar.edu/cas/catalog/climind/soi/html)—the sea level pressure difference between Tahiti, French Polynesia, and Darwin, NE Australia—is negative (El Niño) compared with months that the Southern Oscillation Index (SOI) is positive (La Niña). The difference is mostly seen during the austral summer (DJF, December-January-February) when, on average, negative SOI corresponds with nearly 100 mm/month more precipitation than during the same months when SOI is positive. During the rainiest months in the record, rainfall can exceed 500 mm/month above background.

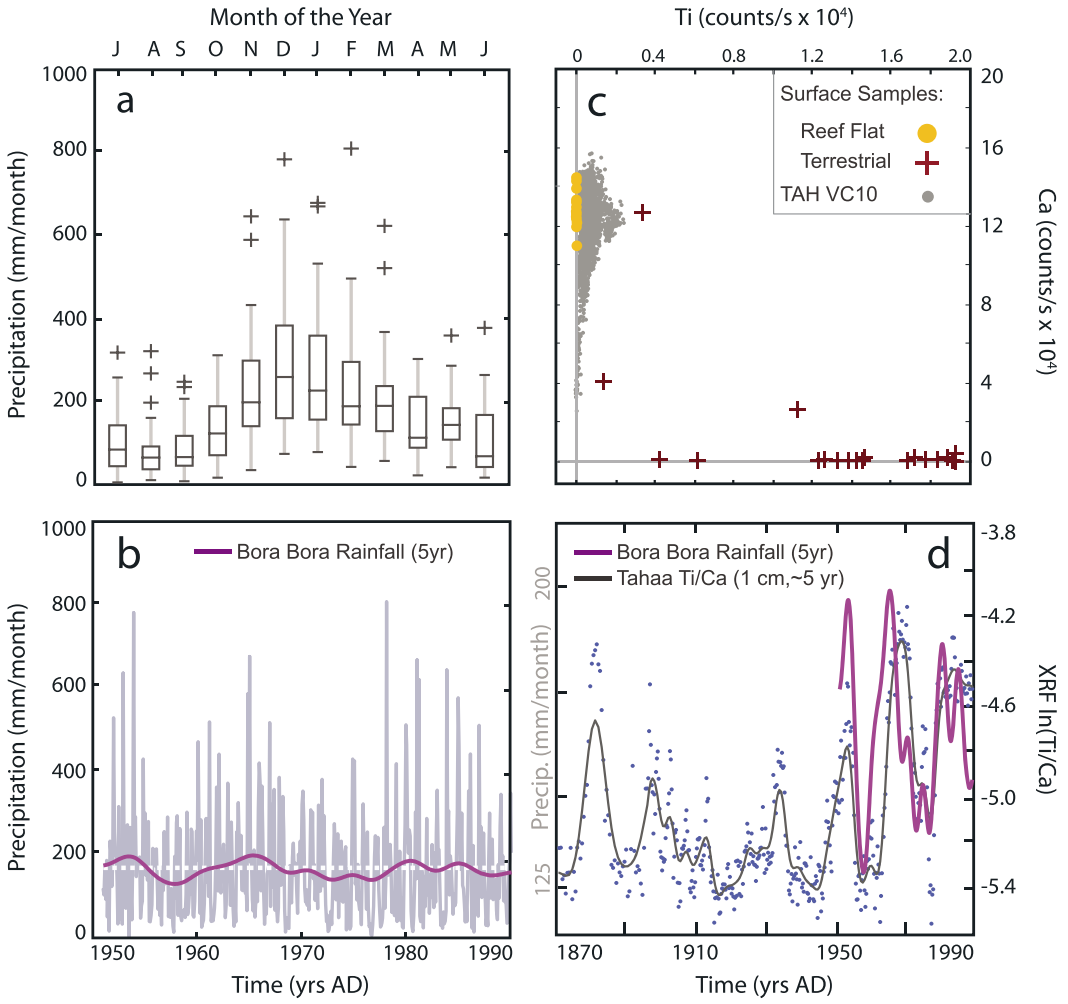

Figure 2. (a) Monthly mean precipitation (KNMI; http://climexp.knmi.nl/) observed for the island of Bora Bora (38 km NW of our site on Tahaa) (1951–2000 C.E.). Cross signs mark statistical outliers. (b) Rain gauge record from Bora Bora. Time series smoothed with 5 year Gaussian filter shown in purple. (c) XRF Ti and Ca counts for discrete surface samples collected from onshore the volcanic island (maroon cross) and reef flat (yellow dot). Grey dots show XRF Ti and Ca intensity for TAH VC10. (d) Ti/Ca time series (blue dots, 1 cm, ~5 year smoothed: grey line) in core top of TAH VC10 based on the highest probability sedimentation ^{210}Pb rate compared to Bora Bora rainfall (5 year smoothed: purple line).

3. Materials and Methods

In January 2009 Common Era (C.E.) we collected a core (TAH VC10) using a Rossfelder P-3 vibracoring system from Apu Bay on the island of Tahaa (17°S 151°W; Figure 1), French Polynesia, 230 km northeast of Tahiti. Seismic profiles (e.g., Figure 1d) were taken using a Benthos CHIRP-II (2–7 kHz). Following recovery, the core was shipped to the Woods Hole Oceanographic Institution (WHOI), split, and refrigerated prior to analysis. Major stratigraphic changes were identified at 10 cm intervals based on measurements of grain size (Beckman-Coulter LS13320), fixed volume dry bulk density and loss on ignition [*Heiri et al.*, 2001] analyses (Table 1).

Higher-resolution (1 cm) downcore grain size changes were measured using standard 63 μm, 250 μm, and 2 mm sieves. Sediment was extracted from the core at 1 cm intervals before being dried at 100°C for 5 h. After the dry mass was obtained, each sample was wet sieved at 63 μm. The >63 μm fraction was then dried and subsequently dry sieved at 250 μm and 2 mm.

Color and mineral properties of the core were measured using optical reflectance spectrometry (Konica Minolta spectrophotometer CM-2600d). Cores were scanned using a Geotek core scanner at 5 mm intervals for wavelengths between 360 and 740 nm (10 nm resolution). We then extracted the primary mineral

Table 1. Major Stratigraphic Changes in Downcore Composition and Grain Size

Depth (cm)	Organic (%)	$CaCO_3$ (%)	d50 Grain Size (μm)	Std. Deviation (μm)	Density (g/cm^3)
5–6	6.2	81.7	24.6	3.0	1.4
15–16	5.9	83.1	26.5	3.0	1.4
25–26	5.6	83.8	27.4	3.3	1.5
35–36	5.6	84.0	26.2	3.1	1.4
45–46	5.7	83.2	24.9	3.1	1.5
55–56	6.2	80.5	25.5	3.1	1.4
65–66	6.2	79.9	24.2	3.1	1.4
75–76	6.3	80.3	24.9	3.2	1.5
85–86	6.0	82.2	24.9	3.2	1.5
95–96	5.9	82.3	24.2	3.2	1.5
105–106	6.2	82.7	19.0	3.0	1.5
115–116	6.2	80.9	19.5	3.1	1.4
125–126	6.1	81.3	19.0	3.0	1.5
135–136	6.0	82.6	24.8	3.3	1.5
145–146	6.0	83.4	23.9	3.3	1.6
155–156	6.0	83.5	18.9	3.5	1.7
165–166	6.1	81.5	22.0	3.4	1.6
175–176	5.9	83.4	23.1	3.4	1.7
185–186	6.0	83.0	20.8	3.2	1.5
195–196	6.1	83.1	23.5	3.4	1.6
205–206	6.0	82.3	22.3	3.4	1.7
215–216	5.9	83.2	22.5	3.5	1.8
225–226	5.7	83.9	23.3	3.4	1.6
235–236	5.7	84.3	23.7	3.4	1.6
245–246	5.9	84.5	18.9	3.5	1.6
255–256	5.0	84.6	23.2	3.4	1.6
265–266	6.9	79.9	12.8	3.6	1.6
275–276	5.2	85.3	19.9	3.5	1.7
285–286	5.1	85.1	19.6	3.4	1.6
295–296	5.2	85.9	22.1	3.7	1.5
305–306	5.2	85.6	22.5	3.5	1.6
315–316	5.0	85.8	21.2	3.7	1.7
325–326	5.0	86.3	22.1	3.5	1.6
335–336	5.2	85.3	22.1	3.6	1.7
345–346	5.1	83.2	21.6	3.5	1.7
355–356	5.2	83.5	23.1	3.8	1.6
365–366	5.0	85.9	21.8	3.7	1.6

constituents from this data: following previously published methods [*Ji et al*., 2005], we (1) computed the first derivative values, (2) determined the principal components, and (3) compared them to the spectral profiles of known minerals in the USGS spectral library (http://speclab.cr.usgs.gov/spectral-lib.html).

In order to estimate the input of terrestrial material downcore we used high-resolution (0.5–1.0 mm) X-ray fluorescence (XRF). Relative elemental abundance measurements were made using ITRAX X-ray fluorescence (XRF) core scanners at WHOI and the University of Massachusetts at Amherst. Core-scanning XRF is ideally suited for this work as it is fast and sensitive to relative changes in metals. The natural logarithm ratio between Ti and Ca was used in part to limit the effects of machine error (e.g., differences in tube strength) and changes in lithology (e.g., grain size, water content, and porosity) on XRF measurements.

Age control in the core was established using ^{210}Pb and radiocarbon dating (Table 2). Measurement of ^{137}Cs did not define a discernable peak in activity related to atmospheric nuclear weapons testing or its subsequent end following the Nuclear Test-Ban Treaty (1963 C.E.). The ^{210}Pb chronology was calculated assuming a constant flux constant sedimentation model [*Appleby and Oldfield*, 1983] as follows: (1) bulk material was extracted from the cores, (2) samples were crushed and homogenized, and (3) ^{210}Pb activity was measured using gamma spectroscopy. We then iteratively (1000 times) resampled the probability distribution for the supported ^{210}Pb levels (~24–30 cm, Figure 3a, light grey dots) and the total error (counting and gamma ray attenuation) on points with excess ^{210}Pb (Figure 3a, black dots) before finding the best linear fit to our log transformed excess ^{210}Pb curve. This produced a distribution of possible maximum apparent accumulation

Table 2. Radiocarbon Dates for Core TAH VC10[a]

Depth (cm)	^{14}C Age (years)	^{14}C Error (years)	ΔR (years)	Material	Method	δ^{13}C ($^{o}/_{oo}$)	Max Prob. Age (years B.P.)
34–35	750	25	225	Bulk Org C	AMS	−16.9	140
80–82	1270	30	225	Bulk Org C	AMS	−17.6	630
119–120	1730	25	225	Bulk Org C	AMS	−17.7	1050
171–172	1930	30	225	Bulk Org C	AMS	−18	1265
196–197	2100	30	225	Bulk Org C	AMS	−17.8	1405
203–205	**3050**	**30**	**225**	**Bulk Org C**	**AMS**	**−19.2**	**2615**
255–257	2370	30	225	Bulk Org C	AMS	−19.2	1720
292–293	2600	25	300	Charcoal	AMS	−28.4	2315
340–342	3130	30	225	Bulk Org C	AMS	−19.4	2705
360–361	3500	30	225	Bulk Org C	AMS	−17.1	3105

[a]The data in bold at 203–205 cm represent a major age reversal and was not used in our age model calculation. ^{14}C Age, 1σ ^{14}C error and *R* are given in radiocarbon years. ^{14}C error is calculated as the larger of the internal statistical error and external reproducibility of the measurement (www.whoi.edu/nosams/radiocarbon-data-calculations). A maximum probable age in years B.P. (1950 C.E.) was calculated for each radiocarbon date using the MARINE13 or SHCal13 calibration curves (5 year resolution) [*Reimer et al*., 2013] and the ΔR value listed here.

rates (Figure 3b), which we then used to generate time series for our runoff record from Tahaa that could be compared to instrumental records of SOI and rainfall. Both instrumental and XRF data were smoothed to 5 year resolution for this procedure.

Conventional Accelerator Mass Spectrometry (AMS) radiocarbon dating of bulk organic material and charcoal was used to develop a long-term chronology for TAH VC10. Measurements were made at the National Ocean Sciences Accelerator Mass Spectrometry facility in Woods Hole, Massachusetts, and Beta Analytic in Miami, Florida. An age model was calculated using ^{14}C dates in three main steps: (1) probability distributions of ΔR-corrected (discussed further below) dates were calibrated following the procedures outlined for Calib 7.1 (http://calib.qub.ac.uk/calib/); (2) the resulting probability distributions were then used to iteratively (10,000 times) generate time index points, then (3) linearly fit between points ending at the ^{210}Pb chronology and assuming superposition, similar to methods developed by *Anchukaitis and Tierney* [2013]. A cubic fit (Figure 3c) could also be used to capture the transitions between a high sedimentation regime from ~1000 to 2000 years B.P. (~2 mm/yr) and slower apparent sedimentation rates prior to 2000 years B.P. (~1 mm/yr), approximately when barrier reefs on nearby Moorea [*Montaggioni*, 2005] and by extension, Tahaa, caught up to SL, as well as after 1000 years B.P., following a 1–2 m SL fall from the mid-Holocene Highstand [*Grossman et al*., 1998] which likely resulted in restriction of the lagoon.

Bulk organic radiocarbon samples (Table 2) from Tahaa show a δ^{13}C signature (−17 to −19‰) consistent with a marine source [*Stuiver and Polach*, 1977] and were calibrated using the Marine13 curve [*Reimer et al*., 2013]. We apply a ΔR of 225 years to these samples consistent with (1) the observed offset between our ^{210}Pb chronology and adjacent radiocarbon dates and (2) radiocarbon dating of deposit feeders from other South Pacific islands [*Petchey et al*., 2008] which likely draw their carbon from a similar ^{14}C pool. A built in age of ~300 years was estimated for a large, single grain, of wood charcoal (292–293 cm) based on the average apparent built-in ages in dated charcoal from archeological sites on the nearby island of Huahine (50 km east) [*Anderson and Sinoto*, 2002]. Preliminary gas bench dates [*von Reden et al*., 2012] made on detrital carbonate were not used due to a large apparent offset ($\Delta R > 1000$ radiocarbon years) likely due to the reworking of old material from nearby relic Pleistocene fringing reefs.

4. Proxy Development

Color changes in the sediment core, seen using reflectance spectrophotometry, indicate that terrestrial material is periodically mobilized from the adjacent volcanic slopes during heavy rainfall events and deposited in the lagoon. Principal component analysis of reflectance peaks suggests that Ti-oxides (Figure 4e) constitute a significant component of the sediments and correspond to visible red-brown streaks (centimeter scale) in the core. Previous work in the Society Islands chain documents Ti-oxides (e.g., ilmenite and rutile) as significant components of soils (Tahiti: 3–4%) [*Parkes et al*., 1992] and the volcanic basement rocks (2–3%) at Tahaa [*Schiano et al*., 1992]. Heavy mineral components typical of ocean island basalts (olivine and pyroxenes)

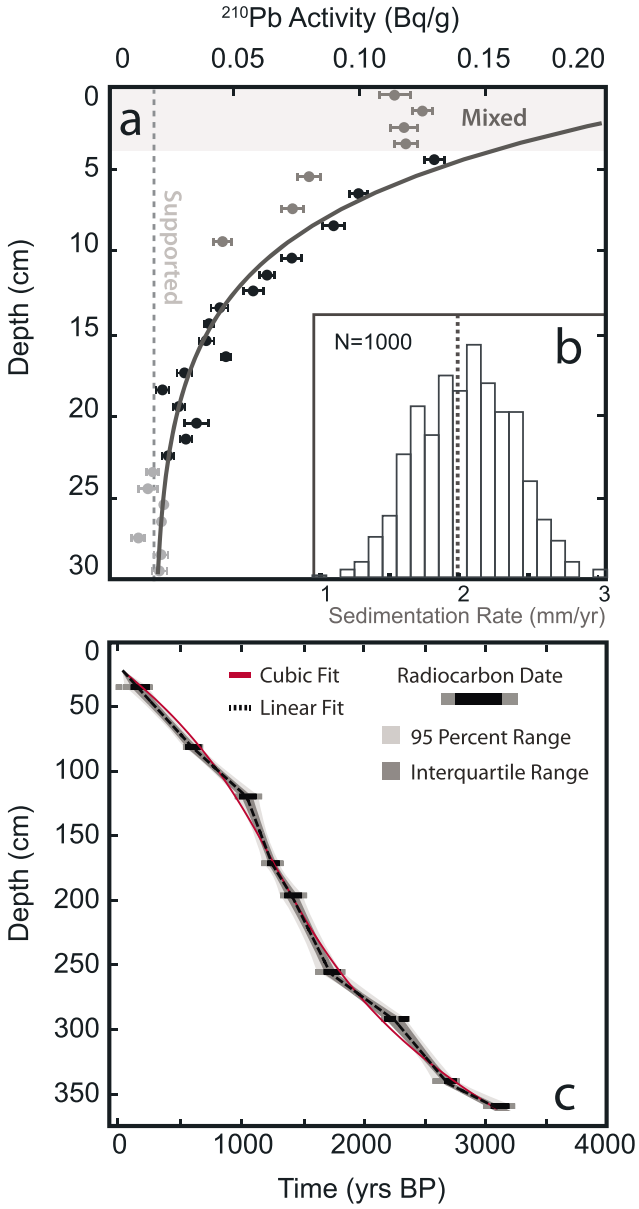

Figure 3. ^{210}Pb and radiocarbon chronology for TAH VC10. (a) Top gives ^{210}Pb profile for upper 30 cm of TAH VC10. Circles and error bars show the measured ^{210}Pb activity and 1 sigma error range. Solid grey line shows the mean sedimentation rate. Medium grey circles (shaded grey area) are likely mixed and were not used in calculating our age model. Grey dashed line indicates level of supported ^{210}Pb in the sediments. (b) Inset shows a histogram of probable sedimentation rates generated by resampling the uncertainty on ^{210}Pb measurements 1000 times. (c) Mean chronology and errors for the radiocarbon chronology of TAH VC10. Bars indicate 1 sigma (black) and 2 sigma (grey) ranges for corrected radiocarbon dates.

are lacking in TAH VC10 sediments, likely reflecting transport limitations. The matrix material is made up of grey carbonate mud (e.g., bioeroded fragments and aragonite needles) and glauconite (green) produced in situ or on the reef. Coarse material in the core is dominantly detrital carbonate (e.g., shell fragments and worm tubes), likely swept off nearby reefs during storms. Together, this evidence suggests that soil material is episodically delivered to the lagoon, deposited into sediments that are otherwise dominated by carbonate mud and may be used to reconstruct a record of precipitation back through time.

Comparison of Ti and Ca intensities from discrete soil samples collected on Tahaa and carbonate material taken from the reef flat (Figure 2c) demonstrates a clear elemental division between these end-members. Carbonate reef material is depleted in titanium whereas terrestrial samples contain little calcium. Likewise, downcore increases in ln(Ti/Ca) XRF intensities—an approximation of actual log ratios of elemental concentrations which sensitivity studies indicate have an error of a few percent [e.g., *Weltje and Tjallingii*, 2008]—closely track red sediment color (Figure 4b), consistent with deposition of Ti-oxides and other volcanic weathering products. Therefore, we interpret titanium-rich material recovered from Apu Bay (Figures 2d and 5b) as terrestrially derived.

Covariance (Figure 4b) of upland runoff (Ti-oxide) relative to both glauconite (a*, which is insensitive to changes in the amount of white, carbonate, sediment) and carbonate material (XRF ln(Ti/Ca), which is insensitive to glauconite $(K,Na)(Fe^{3+},Al,Mg)_2(Si,Al)_4O_{10}(OH)_2$ effectively reduces TAH VC10 sediments to a two-component (terrestrial/marine) system. Changes in XRF ln(Ti/Ca), referred to as Ti/Ca from now on, could potentially result from variable deposition of either the lagoon-derived (carbonate + glauconite + marine organics) or terrestrial (oxides + terrestrial organics) component. Comparison of XRF Ti intensity in TAH VC10 to soil samples (~2.5%, Figure 2c), suggests that upland-derived material makes up only a small fraction of the core, in line with measurement of HCl burn insoluble residues (≤5% weight).

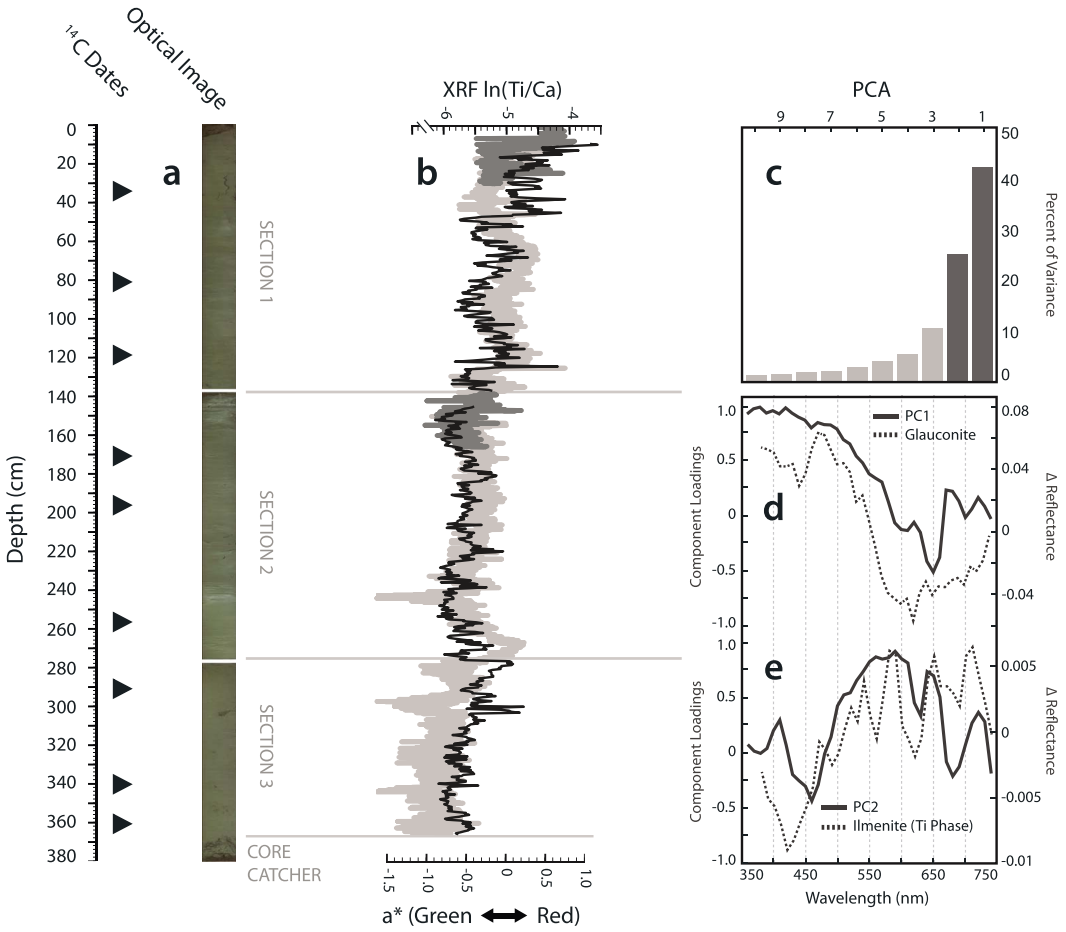

Figure 4. Color and principal component analysis of optical spectrophotometry data for TAH VC10. (a) Color image. Triangles show depth of ^{14}C index points (Table 2). (b) Comparison of a* to XRF-derived ln(Ti/Ca) data (a* is a standard metric of the red to green color ratio of the sediments [*Blum*, 1997]). Reflectance spectroscopy is insensitive to changes in carbonate (white) material. (c) Scree plot showing the percent of variance accounted for by each principal component. First two principal components are marked by dark grey bars. (d) Comparison of Δ Reflectance for first principal component (grey) and glauconite (dashed) using data (interpolated to 10 nm spacing) from the USGS spectral reflectance library [*Clark et al*., 2007]. (e) Comparison of Δ Reflectance for second principal component (grey) and ilmenite (dashed). Core tops (~10 cm) of sections 1 and 2 were not used for spectral analysis due to possible disturbance during shipment. Intact areas of the core were subsampled using U-channels and scanned again separately for XRF analysis (medium grey shading in Figure 4b).

Increased downcore density (Table 1), correlated to sediment grain size standard deviation (sorting/porosity) and changes in sedimentation rate are therefore likely driven by variable delivery of marine material which comprises upward of 90% of TAHVC10 sediments. However, if concentration or dilution of Ti-oxides were dominating the XRF Ti/Ca signal, we would expect it to be inversely related to sedimentation rate, which it is not. For example, background XRF Ti/Ca increases and wt % $CaCO_3$ decreases from the bottom of the core through 145 cm despite sedimentation increasing and minimal change in bulk density. Likewise, the large increase (~4 times) in Ti oxides between ~125 (>1200 XRF Ti counts/s) and 145 cm (~300 counts/s), occurs when sedimentation is high and there is relatively little change in density (~5–7%). This transition (~1300–1000 years B.P.) to increased terrestrial deposition also predates the likely arrival of Polynesian settlers to the Society Islands (~925–830 years B.P.) [*Wilmshurst et al*., 2011]. Well-dated archeological remains on nearby Huahine (50 km east) cluster around ~750 years B.P. [*Anderson and Sinoto*, 2002] suggesting a lag of several centuries between colonization and the eventual buildup of substantial human settlements in the Leeward Society Islands. Several other large magnitude changes in Ti/Ca also occur over the past 1000 years (e.g., ~400 years B.P.) and are unaccompanied by major changes in density,

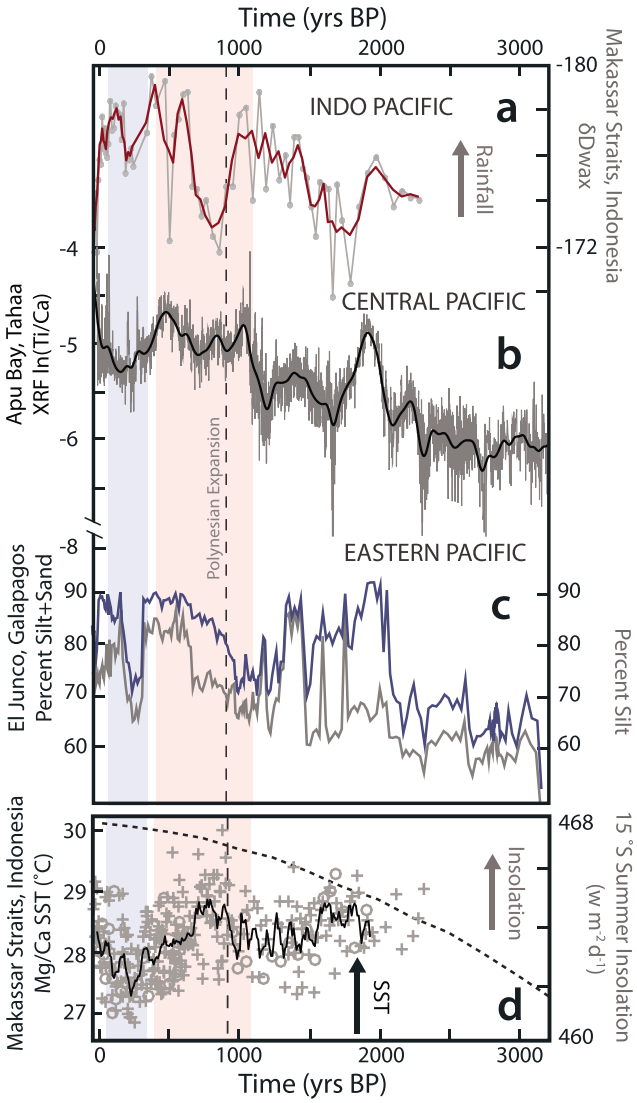

Figure 5. Long-term changes in tropical Pacific precipitation during the late Holocene. (a) δD_{wax} precipitation proxy data from the Indo-Pacific Warm Pool [*Tierney et al.*, 2010]. Raw data are given by grey line, while red line shows the three-point moving average. (b) Ti/Ca ratios over the past 3200 years recorded in sediments from Apu Bay, Tahaa. Black line shows 100 year Gaussian filter of Ti/Ca data (medium grey). (c) Changes in silt-sized and silt + sand grain size fraction observed from El Junco Lake, Galapagos [*Conroy et al.*, 2008]. (d) Fifty year composite IPWP SST (Mg/Ca) given by black line. Raw data shown in grey [*Oppo et al.*, 2009]. Grey dashed line shows the calculated daily, austral summer (NDJF) incoming solar radiation at 15°S (http://www.people.fas.harvard.edu/~phuybers/Mfiles/Toolbox/). Blue and red shading highlight periods of increased rainfall or drought over zthe past ~1000 years. Thin dashed line shows earliest probable migration of Polynesians into French Polynesia [*Wilmshurst et al.*, 2011].

sedimentation, or macroscopic charcoal deposition potentially related to land clearance. Therefore, we suggest that variable Ti/Ca in TAH VC10 is largely driven by the deposition of Ti-oxides related to changes in rainfall, not marine sedimentation or human disturbance.

Delivery of upland material to the lagoon likely represents a threshold process with generation of overland flow requiring soil saturation and sustained heavy rainfall. Volcanic rocks/soils typically have high infiltration capacity, and surface runoff may occur during only a small subset of strong storms [*Peterson*, 1972]. Peaks in Ti/Ca likely represent episodic delivery of terrestrial material by heavy rainfall, predominantly during the austral summer (DJF), which are then smoothed (~5–10 years) by mixing processes at the seafloor. Mean background rainfall conditions may modulate centennial scale changes in terrestrial sediment supply to the lagoon by pacing groundwater recharge and therefore chemical weathering rates [*Schopka and Derry*, 2012].

Extreme precipitation during passage of tropical systems can also result in runoff/extreme flooding [*Galewsky et al.*, 2006; *Silverberg et al.*, 2007]; however, instrumental observations from Bora Bora (Figures 2a and 2b) show that storms also commonly produce little change in rainfall near our site. For example, precipitation for November 1997 C.E. totaled only 262 mm despite a direct strike by Osea (CAT 2), the closest cyclone to pass our site during the instrumental era (>1950 C.E.) [*Knapp et al.*, 2010]. Three of the seven tropical systems to pass within 100 km of the Bora Bora rain gauge station (>1950 C.E.) occurred during December (Lisa, TS) February, and March (Prema, TD; Rewa, CAT 3) of 1982/1983 C.E., but rainfall levels during these months (356, 213, and 122 mm, respectively) diverge little from their monthly means (Figure 2a). However, disturbance (tree mortality/fires) of coastal forests due to intense storm strikes [*Walker*, 1991; *Whigham et al.*, 1991] could promote runoff under conditions of comparable rainfall. Large charcoal fragments (~5 mm diameter), likely indicating significant fires, were found between ~292–293 and 334–335 cm in TAH VC10.

5. Results and Discussion

5.1. Pacific Rainfall Variability

The derived record of terrestrial runoff at our site demonstrates a strong correspondence to observed changes in historic local rainfall. In general, we observe an increase in Ti/Ca after 1950 C.E. which likely corresponds with three periods (~1950–1954, 1960–1967, and 1979–1988 C.E.) of increased rainfall at Bora Bora. Likewise, we see episodes of higher rainfall around 1900 C.E., consistent with observational records showing several large negative SOI excursions around this time. However, we note that Tahaa is located just to the northeast of the nodal region for historic El Niño–Southern Oscillation (ENSO) SST/wind variability which potentially tempers its sensitivity to changes in rainfall related to SOI. Of the thousand potential sedimentation rates (Figure 3b) generated by resampling the uncertainties in our ^{210}Pb chronology, more than 88% yield a negative correlation (Pearsons "*r*") between Ti/Ca and SOI, although only a small subset (~16%) are significant at the $p < 0.1$ level after taking into account autocorrelation of the time series [*Ebisuzaki*, 1997]. While the short length of instrumental records and the effective resolution of TAH VC10 core top (~5 years, Figures 2 and 3) limit statistical comparisons, the recent depositional history of Ti/Ca in TAH VC10 nonetheless suggests that downcore changes in Ti/Ca reflect the variability of precipitation at Tahaa (Figure 2d) which has been influenced by the SPCZ during the historic and geologic past.

Over the late Holocene, substantial changes in runoff at Tahaa have occurred on millennial to decadal time scales, likely driven by different climatic forcings (Figure 5). Gradual intensification in background precipitation is seen across French Polynesia over the late-Holocene, potentially reflecting precessional forced SPCZ migration and/or intensification. Increased runoff over the late Holocene is consistent with records from Mangaia (~900 km SW, Cook Islands [*Ellison*, 1994; *Kirch*, 1996]) and Rimatara (~700 km south, Austral Islands [*Prebble and Wilmshurst*, 2009]) which show increased delivery of upland material to lowland swamps in advance of likely Polynesian settlement of French Polynesia (~925–830 years B.P.) [*Wilmshurst et al*., 2011]. These observations may imply an insolation-driven (precession) displacement of the SPCZ. In modeling experiments (PMIP2), decreased austral summer (DJF) insolation during the mid-Holocene (Figure 5d) results in the SPCZ occupying a more southwestern mean position away from French Polynesia [*Braconnot et al*., 2007; *Brown et al*., 2008; *Mantsis et al*., 2013]. Heavier rainfall at sites in both the Indo-Pacific Warm Pool (IPWP) [*Tierney et al*., 2010] (Figure 5a) and Eastern Equatorial Pacific (EEP) [*Conroy et al*., 2008] (Figure 5c) since the mid–late Holocene would seem to exclude simply a transition to more "El Niño-like" conditions. Observed rainfall patterns would, however, be consistent with intensification of rainfall during the austral summer when the ITCZ/SPCZ typically migrates closest to these sites. Runoff records such as those shown in Figure 5 could be particularly sensitive to the latter with more intense rainfall increasing the likelihood of generating overland flow.

Centennial scale variability in runoff at Tahaa (Figure 5b) may in part be influenced by global temperature changes (e.g., the Little Ice Age/Medieval Climate Anomaly) [*Mann et al*., 2008] and zonal SST gradients in the equatorial Pacific [*Conroy et al*., 2010], with increased (decreased) rainfall between ~1000 and 400 years B.P. (400 and 100 years B.P.). Mechanistically, strong (weak) zonal Pacific SST gradients are associated with expansion (contraction) of the SPCZ and stronger (weaker) convection [*Brown et al*., 2012; *Widlansky et al*., 2011]. Mg/Ca-based reconstructions from the Makassar Strait indicate a decrease (~1–2°C) in IPWP SST around 350 years B.P. [*Oppo et al*., 2009], potentially signaling a weakening of Pacific zonal temperature gradients. Decreased precipitation at Tahaa (Figure 5b) between ~1550 and 1850 C.E. is consistent with a coral-based reconstruction from Rarotonga and Fiji that indicates an expansion of the SPCZ since ~1800 C.E. [*Linsley et al*., 2006]. A stalagmite-reconstructed rainfall record from Vanuatu also suggests a slight intensification of background rainfall since the end of the Little Ice Age [*Partin et al*., 2013].

Evaluation of the standard deviation of our Ti/Ca record using a 100 year sliding window indicates abrupt changes in runoff at decadal time scales also occurred between ~2800–1600, 1300–1000, and 300 years B.P. to present (Figure 6). By analogy to the historic period of our record (Figure 2d), these peaks may represent deposition during decadal scale increases in large rainfall events. Decadal scale variability from 2800 to 1600 years B.P. at Tahaa appears comparable to coarse runoff deposits in cores from El Junco Lake, Galapagos (~675 meters above sea level—m asl) [*Conroy et al*., 2010], but the opposite of runoff deposits at Laguna Pallcacocha (~4200 m asl), Ecuador [*Moy et al*., 2002] (Figure 6). Both EEP records have previously been interpreted as reflecting increased El Niño event frequency but like most runoff records, including our

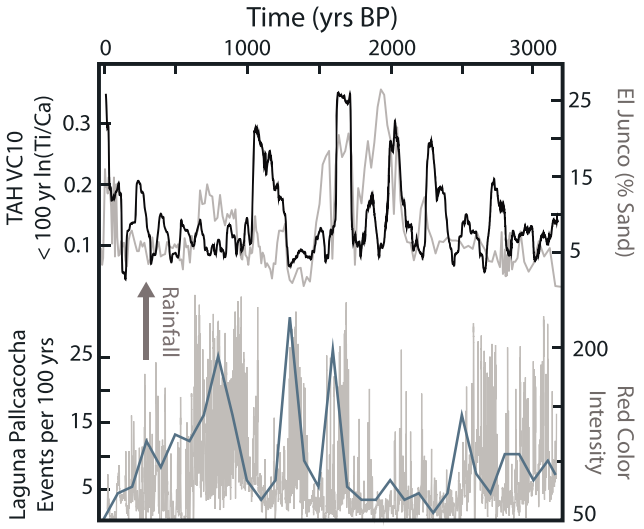

Figure 6. High-frequency runoff variability. (top) Standard deviation of Tahaa Ti/Ca record, smoothed to 1 cm resolution, within 100 year sliding window shown in black. El Junco sand fraction [*Conroy et al*., 2008] given by grey line. (bottom) A record of red color intensity from Laguna Pallcacocha, Ecuador [*Moy et al*., 2002]. Increased red color intensity is inferred to relate to increased runoff.

own, likely integrate several modes of hydroclimate variability. NCEP/NCAR reanalysis of 500 mb winds (1971–2000 C.E.) [*Kistler et al*., 2001; *Whitlock et al*., 2007] suggests winds reaching the high Andes (Ecuador) today largely originate from the tropical Atlantic, with only a very moderate relationship of rainfall to ENSO [*Mora and Willems*, 2012] near Laguna Pallcacocha. *Van Hengstum et al*. [2016, and references therein] suggest that runoff at Laguna Pallcacocha may be related to ITCZ variability, consistent with Caribbean vegetation/rainfall records and phasing of North Atlantic hurricane activity, which is enhanced when the northern edge of the ITCZ migrates toward the Main Development Region (~20–80°W, 10–20°N). A more compressed (extensive) seasonal range of the ITCZ around the equator during periods of low (high) multidecadal Pacific SST variability could potentially explain the apparent anticorrelation of the Laguna Pallcacocha record and high-frequency Ti/Ca variability at Tahaa. Episodes of abrupt change in runoff at Tahaa also bear some similarity to a composite record of "SOI" from proxy records throughout the Pacific [*Yan et al*., 2011], but we note that the resolution of both our record and many of those used by *Yan et al*. [2011] does not permit characterization of variability at ENSO time scales (2–7 years), nor do they directly measure the changes in sea surface temperature (SST) or atmospheric pressure associated with ENSO events. Indeed, coral-derived $\delta^{18}O$ (SST) records, with much finer temporal resolution show a considerably different pattern of ENSO evolution over the late Holocene [*Cobb et al*., 2003, 2013].

5.2. Tropical Cyclone Variability

In order to understand how the changes in atmospheric dynamics noted above may have impacted storm activity in the central South Pacific, we used grain size changes in TAH VC10 to reconstruct a record of tropical cyclone strikes at Tahaa (Figure 7c). During intense cyclone landfalls on reef-bound islands, storm waves mobilize coarse sediment, sometimes as large as boulders [*Blumenstock*, 1958; *Harmelin-Vivien*, 1994; *Scoffin*, 1993] on barrier/fore reefs and transport it lagoonward. With fetch between ~1 and 5 km into Apu Bay, generation of waves in the lagoon by strong winds from the south may also transport coarse sediment to the TAH VC10 core site from nearby fringing reefs. Strong currents and flushing of fine sediment out of reef passes during storms [e.g., *Davis*, 1928] may also winnow lagoonal sediments; however, we do not find stratigraphic evidence of significant erosion or depositional hiatuses in TAH VC10.

Given that our site is relatively sheltered (Figure 1c) and southward facing, away from any active margins likely to generate teleseismic tsunamis, we expect that grain size changes in TAH VC10 mostly reflect strong storms passing to Tahaa's east. The coarsest (2.1% $>$ 250 μm) high-energy event deposit of the historic period, dating to the early nineteenth century, may correlate to an 1831 C.E. event which caused large-scale devastation to nearby Bora Bora [*Teissier*, 1982]. A much smaller peak (0.5% $>$ 250 μm) may be associated with Rewa (CAT2, 1983 C.E.), the strongest storm of the instrumental era to pass near Tahaa ($<$100 km), and suggests that the TAH VC10 record largely reflects the frequency of closely passing major cyclones ($\geq$CAT 3). Deeper, we find that coarse-grained deposits in TAH VC10 (~2600–1500 and 900–500 years B.P.) match well with large overwash events in previously developed back-barrier overwash records from Tahaa and dated massive reef block/conglomerate deposits from the Leeward Islands [e.g., *Pirazzoli and Montaggioni*, 1988; *Toomey et al*., 2013, and references therein].

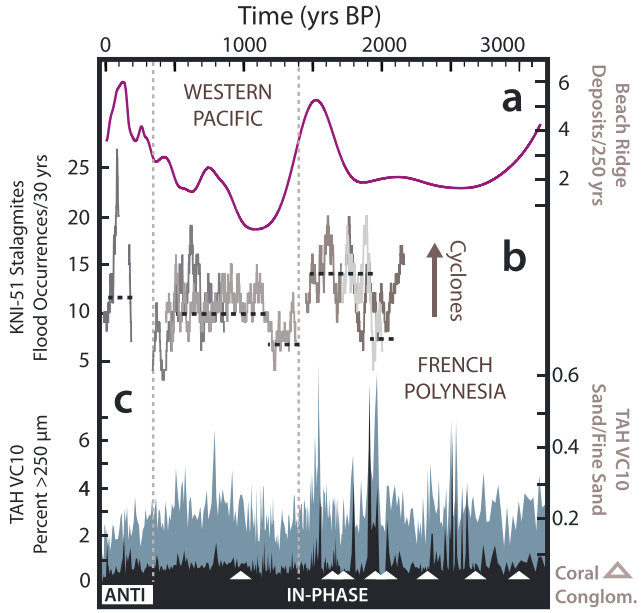

Figure 7. South Pacific storm reconstructions. (a) Composite sequence of beach ridge deposits from Northeastern Australia [*Forsyth et al.*, 2010, 2012; *Nott et al.*, 2009; *Toomey et al.*, 2013]. (b) Tropical cyclone-related flood events in Northern Australia [*Denniston et al.*, 2015]. (c) Record of high-energy event deposition at Tahaa. Black shading shows >250 μm sieve fraction in TAH VC10. Blue shading shows the medium (250 μm to 2 mm) sand fraction normalized by the fine (63 μm–250 μm) sand fraction, which is assumed to relate to the transport competency of fair-weather waves which has likely varied in response to late Holocene sea level changes [*Grossman et al.*, 1998].

In order to evaluate the correlation between grain size (medium/fine sand in TAH VC10) and Ti/Ca (interpolated/smoothed to the 1 cm resolution of our grain size measurements) we compared our data to 10,000 time series with the same spectral properties [*Ebisuzaki*, 1997]. This procedure yielded a weak negative correlation (Pearson's $r = -0.15$) that was not significant ($p = 0.29$), indicating little if any relationship between precipitation changes at Tahaa, likely driven by the mean position of the SPCZ and storm activity over the late Holocene. In contrast, increased tropical cyclone activity and high-frequency Ti/Ca variability overlap between ~2600 and 1600 years B.P., potentially analogous to modern observations showing northward migration and zonal orientation of the SPCZ fosters cyclone activity around French Polynesia during strong El Niño events [*Vincent et al.*, 2011].

The similarity between western South Pacific storm proxy records, namely, beach ridge formation [*Forsyth et al.*, 2010, 2012; *Nott et al.*, 2009] and flooding [*Denniston et al.*, 2015] in Northern Australia (Figures 7a and 7b) and overwash records from Tahaa, however, stands in contrast to instrumental records that suggest storm genesis shifts from the western to central South Pacific, coordinated by ENSO phase. A potential source of this dissonance is that South Pacific tropical cyclone activity may itself play an important [*Fedorov et al.*, 2010] but, at present, poorly resolved role in regulating tropical Pacific climate on longer time scales. The historical period, over which tropical cyclone activity in the central South Pacific has been minimal, may therefore be insufficient for assessing the risk of small Pacific islands to tropical cyclone strikes in a warming future.

5.3. Climate Variability and Polynesian Expansion

Changing South Pacific climate conditions of the past three millennia may have also influenced early Polynesian migratory patterns. Many hypotheses have been suggested to resolve the "Long-Pause," a ~1000 year gap between Polynesian expansion into Western Polynesia (~2200–2000 years B.P.) and their eventual colonization of French Polynesia/Remote Polynesia (French Polynesia, ~925–830 years B.P.; Remote Polynesia (i.e., Hawaii, New Zealand, and Rapa Nui, ~760–660 years B.P. [*Anderson et al.*, 2006; *Wilmshurst et al.*, 2011]), including opportunistic voyaging, advances in seafaring/navigation, and simply an incomplete archeological record [e.g., *Kirch*, 2000]. Climatic and oceanographic conditions, however, may also be a factor. Previous authors [*Anderson et al.*, 2006] have advocated that El Niño-like weakening or reversal of easterlies may have aided Polynesian expansion into the central Pacific. However, given the lack of evidence for major ENSO changes in coral $\delta^{18}O$ (SST) records over the late Holocene [*Cobb et al.*, 2003, 2013], shifting rainfall patterns related to the SPCZ may provide a viable alternative explanation for Polynesian expansion. We note that the resumption of Polynesian expansion occurs around the same time rainfall increases dramatically near Tahaa and after our proxy data indicate a decline in South Pacific hurricane activity (Figures 5 and 7). Although evolving wind conditions may have provided a means of migration [*Goodwin et al.*, 2014], SPCZ-driven drought in the Western Pacific (Figure 5) could have worked to push Polynesian

expansion into the Central Pacific while decreasing tropical cyclone activity during the past ~1500 years could have led to increased odds of success for long-distance Polynesian voyaging.

6. Conclusions

We show that back-reef sedimentary archives provide a unique opportunity to fill major gaps in our understanding of past climatic change in the tropical Pacific. While development of additional, widely dispersed, runoff records is likely required to conclusively differentiate SPCZ migration versus intensification, our results suggest higher-frequency SPCZ variability may have fostered cyclone development near Tahaa between 2600 and 1600 years B.P. Changes in both fresh-water availability and tropical cyclone activity may have played a key role in driving Polynesian expansion and will greatly factor into the sustainability of low-lying island communities in the central South Pacific over the coming decades.

Acknowledgments

We would like to thank Andrea Hawkes, Jon Woodruff, Stephanie Madsen, Richard Sullivan, and the crew of the SSV *Robert C. Seamans* for their assistance with core collection and lab work. We appreciated the helpful feedback on earlier versions of this manuscript from Delia Oppo, Taylor Perron, Andrew Ashton, Bill Curry, and Kris Karnauskas as well as thoughtful reviews by Gavin Dunbar, Christopher Charles, and an anonymous reviewer. This project was supported by the WHOI Coastal Ocean and Ocean and Climate Change Institutes as well as a Distinguished Jackson School Postdoctoral Fellowship to Michael Toomey. Data presented here are included as a supporting information.

References

Anchukaitis, K. J., and J. E. Tierney (2013), Identifying coherent spatiotemporal modes in time-uncertain proxy paleoclimate records, *Clim. Dyn.*, *41*(5–6), 1291–1306.

Anderson, A., and Y. H. Sinoto (2002), New radiocarbon ages of colonization sites in East Polynesia, *Asian Perspect.*, *41*(2), 242–257.

Anderson, A., J. Chappell, M. Gagan, and R. Grove (2006), Prehistoric maritime migration in the Pacific islands: A hypothesis of ENSO forcing, *Holocene*, *16*(1), 1–6.

Appleby, P. G., and F. Oldfield (1983), The assessment of ^{210}Pb data from sites with varying sediment accumulation rates, *Hydrobiologia*, *103*(1), 29–35.

Blum, P. (1997), Physical properties handbook: A guide to the shipboard measurement of physical properties of deep-sea cores, *Tech. Note 26*, Ocean Drilling Program, College Station, Tex.

Blumenstock, D. I. (1958), Typhoon effects at Jaluit atoll in the Marshall Islands, *Nature*, *182*, 1267–1269.

Braconnot, P., B. Otto-Bliesner, S. Harrison, S. Joussaume, J.-Y. Peterchmitt, A. Abe-Ouchi, M. Crucifix, E. Driesschaert, T. Fichefet, and C. Hewitt (2007), Results of PMIP2 coupled simulations of the mid-Holocene and Last Glacial Maximum–Part 1: Experiments and large-scale features, *Clim. Past*, *3*(2), 261–277.

Brown, J., M. Collins, A. Tudhope, and T. Toniazzo (2008), Modelling mid-Holocene tropical climate and ENSO variability: Towards constraining predictions of future change with palaeo-data, *Clim. Dyn.*, *30*(1), 19–36.

Brown, J., A. F. Moise, and F. P. Delage (2012), Changes in the South Pacific Convergence Zone in IPCC AR4 future climate projections, *Clim. Dyn.*, *39*, 1–19.

Clark, R. N., G. A. Swayze, R. Wise, E. Livo, T. Hoefen, R. Kokaly, and S. J. Sutley (2007), USGS digital spectral library splib06a, in *U.S. Geological Survey, Digital Data Series 231*.

Cobb, K. M., C. D. Charles, H. Cheng, and R. L. Edwards (2003), El Niño/Southern Oscillation and tropical Pacific climate during the last millennium, *Nature*, *424*(6946), 271–276.

Cobb, K. M., N. Westphal, H. R. Sayani, J. T. Watson, E. Di Lorenzo, H. Cheng, R. Edwards, and C. D. Charles (2013), Highly variable El Niño–Southern Oscillation throughout the Holocene, *Science*, *339*(6115), 67–70.

Conroy, J. L., J. T. Overpeck, J. E. Cole, T. M. Shanahan, and M. Steinitz-Kannan (2008), Holocene changes in eastern tropical Pacific climate inferred from a Galápagos lake sediment record, *Quat. Sci. Rev.*, *27*, 1166–1180.

Conroy, J. L., J. Overpeck, and J. Cole (2010), El Niño/Southern Oscillation and changes in the zonal gradient of tropical Pacific sea surface temperature over the last 1.2 ka, *PAGES*, *18*(1), 32–34.

Davis, W. M. (1928), *The Coral Reef Problem*, Am. Geogr. Soc., New York.

Denniston, R. F., G. Villarini, A. N. Gonzales, K.-H. Wyrwoll, V. J. Polyak, C. C. Ummenhofer, M. S. Lachniet, A. D. Wanamaker, W. F. Humphreys, and D. Woods (2015), Extreme rainfall activity in the Australian tropics reflects changes in the El Niño/Southern Oscillation over the last two millennia, *Proc. Natl. Acad. Sci. U.S.A.*, *112*(15), 4576–4581.

Donders, T. H., F. Wagner-Cremer, and H. Visscher (2008), Integration of proxy data and model scenarios for the mid-Holocene onset of modern ENSO variability, *Quat. Sci. Rev.*, *27*(5–6), 571–579.

Ebisuzaki, W. (1997), A method to estimate the statistical significance of a correlation when the data are serially correlated, *J. Clim.*, *10*(9), 2147–2153.

Ellison, J. C. (1994), Palaeo-lake and swamp stratigraphic records of Holocene vegetation and sea-level changes, Mangaia, Cook Islands, *Pac. Sci.*, *48*(1), 1–15.

Fedorov, A. V., C. M. Brierley, and K. Emanuel (2010), Tropical cyclones and permanent El Niño in the early Pliocene epoch, *Nature*, *463*(7284), 1066–1070.

Folland, C. K., J. A. Renwick, M. J. Salinger, and A. B. Mullan (2002), Relative influences of the Interdecadal Pacific Oscillation and ENSO on the South Pacific Convergence Zone, *Geophys. Res. Lett.*, *29*(13), 1643, doi:10.1029/2001GL014201.

Forsyth, A. J., J. Nott, and M. D. Bateman (2010), Beach ridge plain evidence of a variable late-Holocene tropical cyclone climate, North Queensland, Australia, *Palaeogeogr. Palaeoclimatol. Palaeoecol.*, *297*(3), 707–716.

Forsyth, A. J., J. Nott, M. D. Bateman, and R. J. Beaman (2012), Juxtaposed beach ridges and foredunes within a ridge plain—Wonga Beach, northeast Australia, *Mar. Geol.*, *307–310*, 111–116.

Galewsky, J., C. Stark, S. Dadson, C. C. Wu, A. Sobel, and M. J. Horng (2006), Tropical cyclone triggering of sediment discharge in Taiwan, *J. Geophys. Res.*, *111*, F03014, doi:10.1029/2005JF000428.

Goodwin, I. D., S. A. Browning, and A. J. Anderson (2014), Climate windows for Polynesian voyaging to New Zealand and Easter Island, *Proc. Natl. Acad. Sci. U.S.A.*, *111*(41), 14,716–14,721.

Grossman, E., C. Fletcher III, and B. Richmond (1998), The Holocene sea-level highstand in the equatorial Pacific: Analysis of the insular paleosea-level database, *Coral Reefs*, *17*(3), 309–327.

Guillou, H., R. C. Maury, S. Blais, J. Cotten, C. Legendre, G. Guille, and M. Caroff (2005), Age progression along the Society hotspot chain (French Polynesia) based on new unspiked K-Ar ages, *Bull. Soc. Geol. Fr.*, *176*(2), 135–150.

Harmelin-Vivien, M. L. (1994), The effects of storms and cyclones on coral reefs: A review, *J. Coast. Res.*, *12*, 211–231.
Heiri, O., A. F. Lotter, and G. Lemcke (2001), Loss on ignition as a method for estimating organic and carbonate content in sediments: Reproducibility and comparability of results, *J. Paleolimnol.*, *25*(1), 101–110.
Ji, J., J. Shen, W. Balsam, J. Chen, L. Liu, and X. Liu (2005), Asian monsoon oscillations in the northeastern Qinghai–Tibet Plateau since the Late Glacial as interpreted from visible reflectance of Qinghai Lake sediments, *Earth Planet. Sci. Lett.*, *233*(1–2), 61–70.
Kirch, P. V. (1996), Late Holocene human-induced modifications to a central Polynesian island ecosystem, *Proc. Natl. Acad. Sci. U.S.A.*, *93*(11), 5296–5300.
Kirch, P. V. (2000), *On the Road of the Winds: An Archaeological History of the Pacific Islands before European Contact*, Univ. of Calif. Press, Berkeley and Los Angeles.
Kistler, R., W. Collins, S. Saha, G. White, J. Woollen, E. Kalnay, M. Chelliah, W. Ebisuzaki, M. Kanamitsu, and V. Kousky (2001), The NCEP-NCAR 50-year reanalysis: Monthly means CD-ROM and documentation, *Bull. Am. Meteorol. Soc.*, *82*(2), 247–267.
Knapp, K. R., M. C. Kruk, D. H. Levinson, H. J. Diamond, and C. J. Neumann (2010), The International Best Track Archive for Climate Stewardship (IBTrACS), *Bull. Am. Meteorol. Soc.*, *91*(3), 363–376.
Le Roy, P., G. Cabioch, B. Monod, Y. Lagabrielle, B. Pelletier, and B. Flamand (2008), Late Quaternary history of the Nouméa lagoon (New Caledonia, South West Pacific) as depicted by seismic stratigraphy and multibeam bathymetry: A modern model of tropical rimmed shelf, *Palaeogeogr. Palaeoclimatol. Palaeoecol.*, *270*(1–2), 29–45.
Linsley, B. K., A. Kaplan, Y. Gouriou, J. Salinger, P. B. deMenocal, G. M. Wellington, and S. S. Howe (2006), Tracking the extent of the South Pacific Convergence Zone since the early 1600s, *Geochem. Geophys. Geosyst.*, *7*, Q05003, doi:10.1029/2005GC001115.
Mann, M. E., Z. Zhang, M. K. Hughes, R. S. Bradley, S. K. Miller, S. Rutherford, and F. Ni (2008), Proxy-based reconstructions of hemispheric and global surface temperature variations over the past two millennia, *Proc. Natl. Acad. Sci. U.S.A.*, *105*(36), 13,252–13,257.
Mantsis, D. F., B. R. Lintner, A. J. Broccoli, and M. Khodri (2013), Mechanisms of Mid-Holocene precipitation change in the South Pacific Convergence Zone, *J. Clim.*, *26*(18), 6937–6953.
Meehl, G. A., J. M. Arblaster, K. Matthes, F. Sassi, and H. van Loon (2009), Amplifying the Pacific climate system response to a small 11-year solar cycle forcing, *Science*, *325*(5944), 1114–1118.
Montaggioni, L. F. (2005), History of Indo-Pacific coral reef systems since the last glaciation: Development patterns and controlling factors, *Earth Sci. Rev.*, *71*(1–2), 1–75.
Mora, D., and P. Willems (2012), Decadal oscillations in rainfall and air temperature in the Paute River Basin—Southern Andes of Ecuador, *Theor. Appl. Climatol.*, *108*(1-2), 267–282.
Moy, C. M., G. O. Seltzer, D. T. Rodbell, and D. M. Anderson (2002), Variability of El Niño/Southern Oscillation activity at millennial timescales during the Holocene epoch, *Nature*, *420*(6912), 162–165.
Nott, J., S. Smithers, K. Walsh, and E. Rhodes (2009), Sand beach ridges record 6000 year history of extreme tropical cyclone activity in northeastern Australia, *Quat. Sci. Rev.*, *28*(15), 1511–1520.
Oppo, D. W., Y. Rosenthal, and B. Linsley (2009), 2,000-year long temperature and hydrology reconstructions from the Indo-Pacific Warm Pool, *Nature*, *460*, 1113–1116.
Parkes, A., J. T. Teller, and J. R. Flenley (1992), Environmental history of the Lake Vaihiria Drainage Basin, Tahiti, French Polynesia, *J. Biogeogr.*, *19*(4), 431–447.
Partin, J., T. Quinn, C. Shen, J. Emile-Geay, F. Taylor, C. Maupin, K. Lin, C. Jackson, J. Banner, and D. Sinclair (2013), Multidecadal rainfall variability in South Pacific Convergence Zone as revealed by stalagmite geochemistry, *Geology*, *41*(11), 1143–1146.
Petchey, F., A. Anderson, A. Zondervan, S. Ulm, and A. Hogg (2008), New marine ΔR values for the South Pacific subtropical gyre region, *Radiocarbon*, *50*, 373–397.
Peterson, F. L. (1972), Water development on tropic volcanic islands—Type example: Hawaii, *Groundwater*, *10*(5), 18–23.
Pirazzoli, P., and L. Montaggioni (1988), Holocene sea-level changes in French Polynesia, *Palaeogeogr. Palaeoclimatol. Palaeoecol.*, *68*(2), 153–175.
Prebble, M., and J. M. Wilmshurst (2009), Detecting the initial impact of humans and introduced species on island environments in Remote Oceania using palaeoecology, *Biol. Invasions*, *11*(7), 1529–1556.
Reimer, P. J., E. Bard, A. Bayliss, J. W. Beck, P. G. Blackwell, C. B. Ramsey, C. E. Buck, H. Cheng, R. L. Edwards, and M. Friedrich (2013), IntCal13 and Marine13 radiocarbon age calibration curves 0–50,000 years cal B.P, *Radiocarbon*, *55*(4), 1869–1887.
Revell, C. G., and S. W. Goulter (1986), South Pacific tropical cyclones and the Southern Oscillation, *Mon. Weather Rev.*, *114*(6), 1138–1145.
Schiano, P., R. Clocchiatti, and J. Joron (1992), Melt and fluid inclusions in basalts and xenoliths from Tahaa Island, Society Archipelago: Evidence for a metasomatized upper mantle, *Earth Planet. Sci. Lett.*, *111*(1), 69–82.
Schopka, H. H., and L. A. Derry (2012), Chemical weathering fluxes from volcanic islands and the importance of groundwater: The Hawaiian example, *Earth Planet. Sci. Lett.*, *339*, 67–78.
Scoffin, T. (1993), The geological effects of hurricanes on coral reefs and the interpretation of storm deposits, *Coral Reefs*, *12*(3), 203–221.
Silverberg, N., E. Shumilin, F. Aguirre-Bahena, A. P. Rodríguez-Castañeda, and D. Sapozhnikov (2007), The impact of hurricanes on sedimenting particulate matter in the semi-arid Bahía de La Paz, Gulf of California, *Cont. Shelf Res.*, *27*(19), 2513–2522.
Stuiver, M., and H. A. Polach (1977), Discussion; reporting of C-14 data, *Radiocarbon*, *19*(3), 355–363.
Teissier, R. (1982), *Les Cyclones en Polynésie Française: 1878, 1903, 1905, 1906*, Société des Études Océaniennes, Papeete.
Tierney, J. E., D. W. Oppo, Y. Rosenthal, J. M. Russell, and B. K. Linsley (2010), Coordinated hydrological regimes in the Indo-Pacific region during the past two millennia, *Paleoceanography*, *25*, PA1102, doi:10.1029/2009PA001871.
Toomey, M. R., J. P. Donnelly, and J. D. Woodruff (2013), Reconstructing mid-late Holocene cyclone variability in the Central Pacific using sedimentary records from Tahaa, French Polynesia, *Quat. Sci. Rev.*, *77*, 181–189.
van Hengstum, P. J., J. P. Donnelly, P. L. Fall, M. R. Toomey, N. A. Albury, and B. Kakuk (2016), The Intertropical Convergence Zone modulates intense hurricane strikes on the western North Atlantic margin, *Sci. Rep.*, *6*, 21728, doi:10.1038/srep21728.
Vincent, D. G. (1994), The South Pacific Convergence Zone (SPCZ): A review, *Mon. Weather Rev.*, *122*(9), 1949–1970.
Vincent, E., M. Lengaigne, C. Menkes, N. Jourdain, P. Marchesiello, and G. Madec (2011), Interannual variability of the South Pacific Convergence Zone and implications for tropical cyclone genesis, *Clim. Dyn.*, *36*(9-10), 1881–1896.
von Reden, K. F., M. L. Roberts, J. R. Burton, and S. R. Beaupre (2012), Optimizing a microwave gas ion source for continuous-flow accelerator mass spectrometry, *Rev. Sci. Instrum.*, *83*(2), 02B304, doi:10.1063/1.3656408.
Walker, L. R. (1991), Tree damage and recovery from Hurricane Hugo in Luquillo experimental forest, Puerto Rico, *Biotropica*, *23*, 379–385.
Weltje, G. J., and R. Tjallingii (2008), Calibration of XRF core scanners for quantitative geochemical logging of sediment cores: Theory and application, *Earth Planet. Sci. Lett.*, *274*(3), 423–438.
Whigham, D. F., I. Olmsted, E. C. Cano, and M. E. Harmon (1991), The impact of Hurricane Gilbert on trees, litterfall, and woody debris in a dry tropical forest in the northeastern Yucatan Peninsula, *Biotropica*, *23*, 434–441.

Whitlock, C., P. I. Moreno, and P. Bartlein (2007), Climatic controls of Holocene fire patterns in southern South America, *Quat. Res.*, *68*(1), 28–36.

Widlansky, M. J., P. J. Webster, and C. D. Hoyos (2011), On the location and orientation of the South Pacific Convergence Zone, *Clim. Dyn.*, *36*(3), 561–578.

Wilmshurst, J. M., T. L. Hunt, C. P. Lipo, and A. J. Anderson (2011), High-precision radiocarbon dating shows recent and rapid initial human colonization of East Polynesia, *Proc. Natl. Acad. Sci. U.S.A.*, *108*(5), 1815–1820.

Xie, P., and P. A. Arkin (1997), Global precipitation: A 17-year monthly analysis based on gauge observations, satellite estimates, and numerical model outputs, *Bull. Am. Meteorol. Soc.*, *78*(11), 2539–2558.

Yan, H., L. Sun, Y. Wang, W. Huang, S. Qiu, and C. Yang (2011), A record of the Southern Oscillation Index for the past 2,000 years from precipitation proxies, *Nat. Geosci.*, *4*(9), 611–614.

Zinke, J., J. J. G. Reijmer, and B. A. Thomassin (2001), Seismic architecture and sediment distribution within the Holocene barrier reef lagoon complex of Mayotte (Comoro archipelago, SW Indian Ocean), *Palaeogeogr. Palaeoclimatol. Palaeoecol.*, *175*(1–4), 343–368.